

Original Article

Construction of cuproptosis-related lncRNAs/mRNAs model and prognostic prediction of hepatocellular carcinoma

Lingxue Tang^{1*}, Tong Wang^{2*}, Wen Li¹, Sheng Yu¹, Senbang Yao¹, Huaidong Cheng¹

¹Department of Oncology, The Second Affiliated Hospital of Anhui Medical University, Hefei 230601, Anhui, China;

²Department of General Medicine, The Second Affiliated Hospital of Anhui Medical University, Hefei 230601, Anhui, China. *Equal contributors.

Received August 8, 2022; Accepted September 15, 2022; Epub October 15, 2022; Published October 30, 2022

Abstract: Cuproptosis is a recently reported novel form of cell death, which is involved in the regulation of tumor progression. However, the specific role of cuproptosis in hepatocellular carcinoma (HCC) development remains unclear. In this study, we comprehensively analyzed the effect of cuproptosis-related lncRNAs/mRNAs on the prognosis of HCC patients based on the RNA-Seq transcriptome data and clinical data. We identified 6 cuproptosis-related signatures by Cox and Lasso regression analysis, including 3 mRNAs (FBXO30, RNF2, MPDZ) and 3 lncRNAs (PICSAR, LINC00426, AL590705.3). In addition, we constructed a prognostic prediction model for HCC. Risk analysis, RT-qPCR, and Kaplan-Meier analysis showed that the expression of FBXO30, RNF2, AL590705.3 and PICSAR was elevated in HCC, while the expression of MPDZ and LINC00426 was suppressed which was associated with better overall survival. Furthermore, immune response analysis suggested that HCC with high-risk score might respond favorably to immunotherapy. Moreover, the potential drugs that HCC might be sensitive to were screened by drug sensitivity profiling analysis. Taken together, our findings provided important information for the prediction of the prognosis of HCC patients and the development of personalized targeted therapy.

Keywords: Cuproptosis, hepatocellular carcinoma, lncRNA, mRNA, prognosis

Introduction

Liver cancer is one of the most common malignant cancers worldwide, with an estimated 900,000 new cases and 830,000 deaths each year, accounting for 4.7% and 8.3% of all malignant cancers, respectively [1]. Hepatocellular carcinoma (HCC) accounts for about 80% of primary liver cancer [2], and the risk factors for HCC include chronic hepatitis (hepatitis B or C virus infection), alcoholism, and metabolic syndrome [3]. The current treatment options for HCC include curative surgery (lesion resection, liver transplantation or local ablation) and supportive care. Although the 5-year survival rate of surgical treatment is as high as 75%, only 20% of patients are eligible for surgery due to the advanced stages at diagnosis, liver dysfunction, or insufficient liver donors. The 3-year survival rate for palliative care is 10-40%, while the prognosis for symptomatic treatment is

poor, with typical patients survival of less than 3 months [4]. Although targeted therapy and immunotherapy have demonstrated promising progress in the treatment of HCC in recent years, the 5-year survival rate is still not satisfactory. Therefore, it is imperative to identify novel strategies for the early diagnosis and the prediction of prognosis.

Cuproptosis is a newly discovered form of non-apoptotic programmed cell death, which is triggered by copper overload and mediated by protein lipidation [5]. Since copper chelators or copper ionophores are considered to play an important role in inhibiting the occurrence and development of cancers [6], they may present as a new opportunity for HCC therapy. Copper is one of the important transition metals required for survival and participates in various physiological processes such as oxygen metabolism, maintenance of iron homeostasis, and neu-

rotransmitter synthesis [7]; however, excess or deficiency of copper is related to many human diseases [8]. Cellular aging, genetic mutation, or environmental influences can cause the disruption of copper homeostasis and lead to a wide range of adverse consequences, such as cancer and neurodegeneration [9, 10]. Accordingly, copper chelation has been shown to be effective in the treatment of Menke's syndrome and Wilson's disease. However, the role of cuproptosis in cancers remains to be fully understood [11]. In a phase III clinical trial of copper ionophore (elesclomol) in the treatment of melanoma, the anticancer effect of elesclomol in patients with low plasma lactate dehydrogenase levels is detected [12]. Nevertheless, there are no reports on the application of cuproptosis in cancer treatment, and the specific mechanism involving the fine regulation of cuproptosis is still unclear.

In this study, a prognostic model was established based on the gene transcription data and clinical data to explore the expression profile, function and biological signaling pathways of cuproptosis-related signature in HCC, and to predict the effectiveness of immunotherapy and potential sensitive drugs. Our results will shed light on the development of targeted drugs, the prognostic prediction, and the selection of treatment strategies for HCC.

Materials and methods

Data collection and preprocessing

The transcriptome data, clinical data and gene mutation data of HCC were downloaded from The Cancer Genome Atlas database (TCGA, <https://portal.gdc.cancer.gov/>). The retrieval strategy was shown in [Supplementary Table 1](#). Perl software was first used to preprocess the downloaded dataset to obtain the matrices of "sample IDs - gene expression levels", "clinical information - sample IDs", and "tumor mutation burden (TMB) - sample IDs". Then, R package "limma" and pre-prepared cuproptosis-related gene files ([Supplementary Table 2](#)) were used to extract the expression levels of cuproptosis-related genes in each sample for further analysis.

Prognostic model construction

We utilized the downloaded clinical data to analyze the survival information of each sample.

Samples with missing information were excluded. R package "limma" was used to integrate the cuproptosis-related lncRNAs/mRNAs data with survival data. Subsequently, we cycled the merged data once and randomly divide them into training group and testing group to construct a prognostic model ($P < 0.05$ was defined as significant correlation). Univariate Cox analysis was performed to identify the prognostic-associated lncRNAs/mRNAs. In addition, the least absolute shrinkage and selection operator (LASSO) analysis was used to select the prognostic signatures and the model formula. Furthermore, we divided the samples into high- and low-risk groups according to the model formula calculated by R software and then compared the differences in overall survival (OS) and progression-free survival (PFS) between these two groups. Finally, time dependent receiver operating characteristic curve (ROC) analysis was carried out to evaluate the predictive validity of the prognostic model.

Production of clinical nomogram

Univariate and multivariate Cox analyses were used to determine whether the clinical characteristics of the prognostic model (age, sex, grade, stage, and risk score) were independent prognostic factors for HCC. Based on the results of the independent prognostic factor analysis, nomograms and calibration curves were plotted using the R packages "regplot" and "rms". Specifically, each prognostic factor was given a score, and the scores of all prognostic factors were added to generate the overall risk score. Then, the overall risk score was used to predict the 1-, 3-, and 5-year survival of HCC, and calibration curve was used to verify the accuracy of the nomogram.

Principal component analysis (PCA)

R packages "scatterplot3d" and "limma" were employed to perform PCA on all genes, all cuproptosis-related genes, all cuproptosis-related lncRNAs/mRNAs, and cuproptosis-related signatures based on HCC dataset. Three-dimensional (3D) scatter plots were created to visualize the results.

Functional and pathway enrichment analysis

R package "limma" and logFC function were used to analyze the differentially expressed genes between the high- and low-risk groups in

Cuproptosis-related signatures predicted prognosis of HCC

HCC. Gene Ontology (GO) and Kyoto Encyclopedia of Genes and Genomes (KEGG) enrichment analyses were performed to identify key genes and pathways involved in HCC. Then, histogram plot, bubble plot and circle plot were generated to visualize the differential gene enrichment in GO function and KEGG pathway. The FDR (< 0.05) correction was used to determine the statistical significance of GO and KEGG results.

Tumor mutational burden (TMB) analysis

TMB is generally defined as the number of non-synonymous mutations presented in a tumor genome. Briefly, we employed Perl software to extract the matrices of “sample IDs - TMB” and “gene IDs - number of mutated samples”, as well as the detailed data on the location and the type of these mutations. Next, based on the risk score, we produced the waterfall plot by using maftools” package to demonstrate the genetic mutations in the high- and low-risk groups. Subsequently, the survival analysis using TMB was performed to determine whether there was a significant difference in TMB between the two groups.

Immune function and drug sensitivity analysis

R packages “limma”, “GSVA”, “GSEABase”, “pheatmap” and “reshape2” were used for immune function analysis, while packages “limma” and “ggpubr” were used for immune exclusion analysis. First, the data on the immune exclusion scores were downloaded from the Tumor Immune Dysfunction and Exclusion (TIDE, <http://tide.dfci.harvard.edu/>). Then, all gene expression data in HCC, cuproptosis-related signature data, TIDE score, and immune function gene sets were visualized by heatmaps and violin plots. Finally, R packages “pRRophetic”, “ggpubr” and “ggplot2” were used to predict the drug sensitivity of HCC.

Cell culture

The normal human liver cell line LO2, liver cancer cell line HepG2 and HuH-7 were purchased from Procell (Wuhan, China). Cell lines were cultured in high-glucose DMEM medium (Gibco, Carlsbad, CA, USA) supplemented with 10% fetal bovine serum (Gibco, Carlsbad, CA, USA) and penicillin (100 IU/ml)/streptomycin (100

$\mu\text{g/ml}$) in a 37°C humidified incubator with 5% CO₂.

RNA extraction and reverse transcription-quantitative PCR (RT-qPCR)

RNA extraction and RT-qPCR were carried out according to the manufacturer’s protocols. Briefly, EasyZol Reagent (NovaBio, Shanghai, China), HyperScript™ III RT SuperMix for qPCR with gDNA Remover (NovaBio, Shanghai, China), and S6 Universal SYBR qPCR Mix (NovaBio, Shanghai, China) were used for cell lysis, cDNA synthesis and RNA detection. Primer sequences used in this study were listed in [Supplementary Table 3](#). The relative expression levels of the target genes were normalized to GAPDH and analyzed by $2^{-\Delta\Delta\text{Ct}}$.

Statistical analysis

R software (v 4.1.3) (<https://www.r-project.org/>) was used for statistical analysis and generating plots. Perl (v 5.30.0) (<https://www.perl.org/>) was used to sort and merge the downloaded data. $P < 0.05$ was considered statistically significant.

Results

Identification of cuproptosis-related lncRNAs/mRNAs

We downloaded a total of 374 tumors and 50 normal samples as well as 59427 gene transcriptome data from TCGA database, which included 16,876 lncRNAs and 19938 mRNAs. Subsequently, we extracted lncRNAs/mRNAs that were co-expressed with cuproptosis-related genes. At the end, we identified 3449 lncRNAs/mRNAs signatures that were co-expressed with the 17 cuproptosis-related genes in HCC, which was visualized by sankey plot (**Figure 1A**).

Construction of prognosis model

We also downloaded the clinical data of 376 HCC samples from TCGA database, including the survival time and survival status. After merging the clinical data with the cuproptosis-related lncRNAs/mRNAs expression data, we selected 370 samples and randomly divided them into the training and the testing groups for model construction. Then, univariate Cox

Cuproptosis-related signatures predicted prognosis of HCC

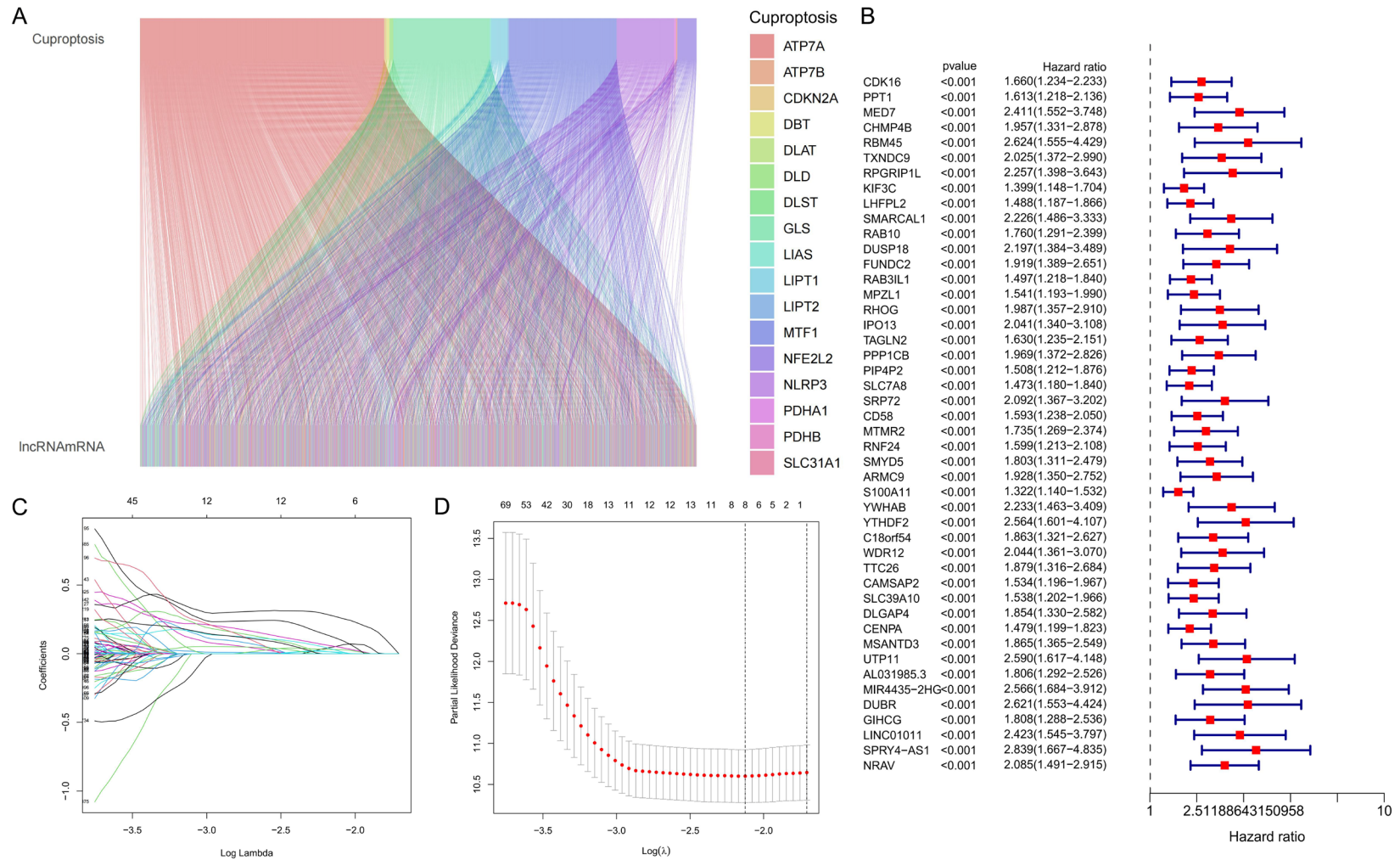


Figure 1. Construction of the prognostic model for HCC. A. Sankey plot of 17 cuproptosis-related genes which were co-expressed with 3449 lncRNAs/mRNAs. B. 532 significantly differentially expressed lncRNAs/mRNAs were screened by univariate Cox analysis in the training group ($P < 0.05$), and 46 of them were shown in the forest plot ($P < 0.001$). C. LASSO regression results of the significantly differentially expressed lncRNAs/mRNAs in HCC. D. A partial likelihood deviation plot of cross validation according to the $\log(\lambda)$. The vertical dotted line indicated the minimum error λ value. The maximal λ value indicated that the deviation was within a standard error range of the minimum value.

analysis was performed on the training group, and a total of 532 lncRNAs/mRNAs significantly associated with prognosis were stratified. We presented the 46 genes with $P < 0.001$ by forest map (**Figure 1B**).

LASSO regression analysis and cross validation were performed to determine the point with minimum error (**Figure 1C, 1D**). Next, we used these signatures to construct a Cox model, and obtained the formula of prognosis model: $FBX030 \times 0.472 + RNF2 \times 0.479 + MPDZ \times (-0.337) + AL590705.3 \times 0.382 + PICSAR \times 0.262 + LINC00426 \times (-1.765)$. Based on the model formula, we calculated the risk scores for each sample in the training and testing groups. According to the median value of the risk scores, we divided the samples into high- and low-risk groups. We found that as the risk score increased, the number of patients who died increased accordingly, and patients at the low-risk group generally had better survival time than those in the high-risk group (**Supplementary Figure 1A, 1B**). In addition, among the 6 optimal lncRNAs/mRNAs, FBX030, RNF2, AL590705.3 and PICSAR were highly expressed in HCC, while the expression of MPDZ and LINC00426 was suppressed (**Figure 2A, 2B**). Importantly, the above conclusions from bioinformatics analysis were validated by the experimental data using RT-qPCR (**Figure 2C, 2D**). It is worth mentioning that the expression levels of MPDZ and LINC00426 were not statistically different in Huh-7. This may be caused by the different sources of HCC cell lines, which may have individual differences in the expression of the same gene. For example, HepG2 was isolated from the primary hepatoblastoma of a Caucasian boy in 1979, and Huh-7 was isolated from the liver cancer tissue of a Japanese male in 1982.

Furthermore, Kaplan-Meier (K-M) analysis was performed for these 6 lncRNAs/mRNAs signatures. The results showed that high expression of FBX030, RNF2, PICSAR, AL590705.3 and low expression of MPDZ, LINC00426 were associated with poor OS in HCC (**Supplementary Figure 1C-H**).

Validation of the prognostic model

We used Chi-square test to compare the baseline clinical characteristics between the train-

ing group and the testing group (**Table 1**). The correlation between the lncRNAs/mRNAs signatures and cuproptosis-related genes in the prognostic model was also analyzed (**Figure 3A**). The K-M analysis results suggested that HCC patients with low-risk scores had better OS (**Figure 3B**) and PFS (**Figure 3D**), which was verified in the testing group (**Figure 3C, 3E**).

In addition, independent prognostic analysis was used to explore whether the prognostic model we constructed could be used as a prognostic factor independent of other clinical characteristics. Univariate and multivariate Cox analyses showed that stage (HR = 1.568, 95% CI = 1.266-1.943; $P < 0.001$) and risk score (HR = 1.150, 95% CI = 1.100-1.203; $P < 0.001$) were independent risk factors for predicting the OS of HCC patient (**Supplementary Figure 2A, 2B**). Furthermore, time dependent-ROC analysis indicated the good predictive value of our prognostic model in predicting 1-, 3- and 5-years OS, with the prediction accuracy of AUC 0.789, 0.822, and 0.749, respectively (**Figure 4A**). Consistently, the predictive power of our prognostic model was superior to clinical predictors such as age, gender, grade, and stage (**Figure 4B**), which was also confirmed in the conformance index analysis (**Figure 4C**).

Development of nomogram to predict OS

For the application of prognostic model in clinical practice, we developed nomograms based on the baseline characteristics and the pathological parameters of HCC. Using this nomogram, the predicted 1-, 3-, and 5-year OS rates for HCC patients were 91.3%, 79.8%, and 67.8%, respectively (**Figure 4D**). And the calibration curve showed that the nomogram had high accuracy (**Figure 4E**).

PCA

PCA was used to verify whether our prognosis model was effective in distinguishing patients between the high- and low-risk groups. We separately analyzed all genes, all cuproptosis-related genes, all cuproptosis-related lncRNAs/mRNAs, and cuproptosis-related signatures in HCC (**Supplementary Figure 3A-D**), and the results showed that our prognostic model accurately differentiated patients between the high- and low-risks.

Cuproptosis-related signatures predicted prognosis of HCC

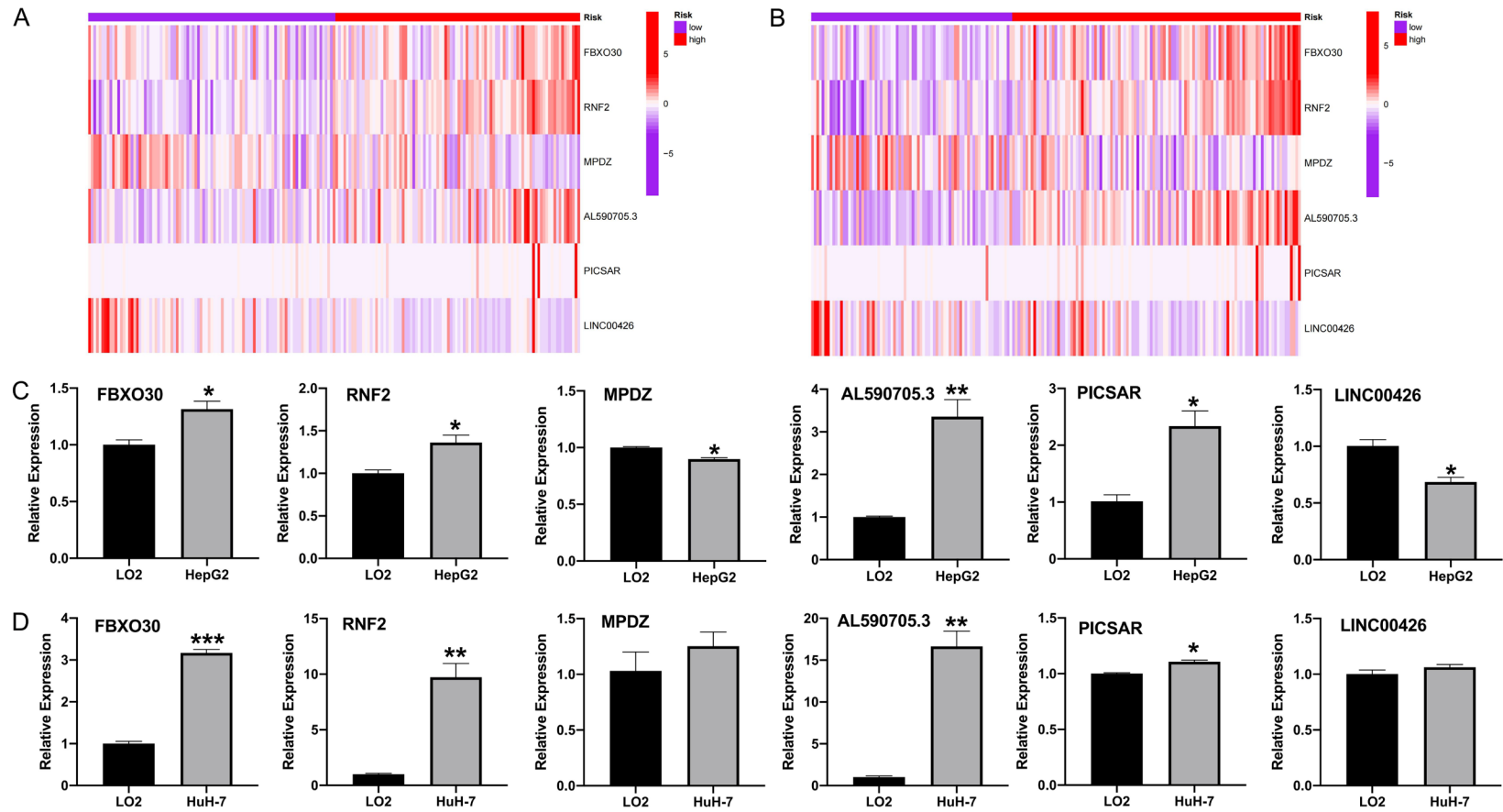


Figure 2. Expression of prognostic signatures and RT-qPCR validation. A, B. FBXO30, RNF2, AL590705.3 and PICSAR were high-risk factors in our prognostic model and in the testing group, while MPDZ and LINC00426 were low risk factors. C, D. RT-qPCR validation for human normal liver cell line LO2, HCC cell lines HepG2 and Huh-7. (* $P < 0.05$, ** $P < 0.01$, *** $P < 0.001$).

Cuproptosis-related signatures predicted prognosis of HCC

Table 1. Baseline characteristics of the training group and testing group

Covariates	Total (%)	Test (%)	Train (%)	p-value
Age				
≤ 65	232 (62.7)	121 (65.41)	111 (60)	0.333
> 65	138 (37.3)	64 (34.59)	74 (40)	
Gender				
Female	121 (32.7)	65 (35.14)	56 (30.27)	0.3753
Male	249 (67.3)	120 (64.86)	129 (69.73)	
Grade				
G1	55 (14.86)	24 (12.97)	31 (16.76)	0.7239
G2	177 (47.84)	87 (47.03)	90 (48.65)	
G3	121 (32.7)	64 (34.59)	57 (30.81)	
G4	12 (3.24)	6 (3.24)	6 (3.24)	
unknow	5 (1.35)	4 (2.16)	1 (0.54)	
Stage				
I	171 (46.22)	82 (44.32)	89 (48.11)	0.3855
II	85 (22.97)	49 (26.49)	36 (19.46)	
III	85 (22.97)	39 (21.08)	46 (24.86)	
IV	5 (1.35)	2 (1.08)	3 (1.62)	
unknow	24 (6.49)	13 (7.03)	11 (5.95)	
T				
T1	181 (48.92)	86 (46.49)	95 (51.35)	0.4508
T2	93 (25.14)	52 (28.11)	41 (22.16)	
T3	80 (21.62)	38 (20.54)	42 (22.7)	
T4	13 (3.51)	8 (4.32)	5 (2.7)	
unknow	3 (0.81)	1 (0.54)	2 (1.08)	
M				
M0	266 (71.89)	134 (72.43)	132 (71.35)	1
M1	4 (1.08)	2 (1.08)	2 (1.08)	
unknow	100 (27.03)	49 (26.49)	51 (27.57)	
N				
N0	252 (68.11)	127 (68.65)	125 (67.57)	1
N1	4 (1.08)	2 (1.08)	2 (1.08)	
unknow	114 (30.81)	56 (30.27)	58 (31.35)	

T = tumor, N = node, M = metastasis.

Functional and pathway enrichment analysis

GO and KEGG enrichment analyses were performed based on the differentially expressed genes (DEGs) in HCC with high- and low-risk scores. Among the three types of GO functions (BP: Biological Process; CC: Cellular Component; MF: Molecular Function), DEGs were mainly enriched in CC and MF, especially in the functions of “external side of plasma membrane”, “collagen-containing extracellular matrix”, “positive regulation of cell activation”, and “positive regulation of leukocyte activation”

(Supplementary Figure 4A-C). Similarly, KEGG enrichment analysis revealed 30 pathways that were significantly associated with DEGs, including PI3K-Akt signaling pathway and pathways of cytokine-cytokine receptor interaction and human papillomavirus infection (Supplementary Figure 4D-F). Together, these results might provide insights into understanding the functions and signaling pathways of cuproptosis-related lncRNAs/mRNAs.

TMB

A total of 372 gene mutation profiles of HCC downloaded from TCGA database were analyzed, and we found that somatic mutations occurred in 143 of 180 (79.44%) samples in the low-risk group and 150 of 181 (82.87%) samples in the high-risk group. The top 15 genes with the highest mutation frequency were shown in the waterfall plots. As shown in Supplementary Figure 5A, 5B, TP53, TTN, MUC16, ALB, RYR2, CSND3, LRP1B and OBSCN were more frequently mutated in the high-risk group, while CTNNB1, PCLO, APOB, ABCA13, ARID1A and HMCN1 were more frequently mutated in the low-risk group. Subsequently, we performed a differential analysis of TMB between the high- and the low-risk groups, and no significant difference was found between the two groups (Supplementary Figure 5C). Furthermore, K-M analysis for TMB showed that patients with low-TMB had better OS outcomes (Supplementary Figure 5D). Lastly, the K-M analysis of TMB combined with risk score showed that patients with low-TMB + low-risk score had the best prognosis, followed by high-TMB + low-risk score and low-TMB + high-risk score, while patients with high-TMB + high-risk score had the worst prognosis (Supplementary Figure 5E).

Prediction of immune response and drug sensitivity

We further performed functional analysis of immune gene sets based on ssGSEA and revealed that our prognostic model was significantly correlated with 10 immune functional pathways, including “Type II IFN response”, “T

Cuproptosis-related signatures predicted prognosis of HCC

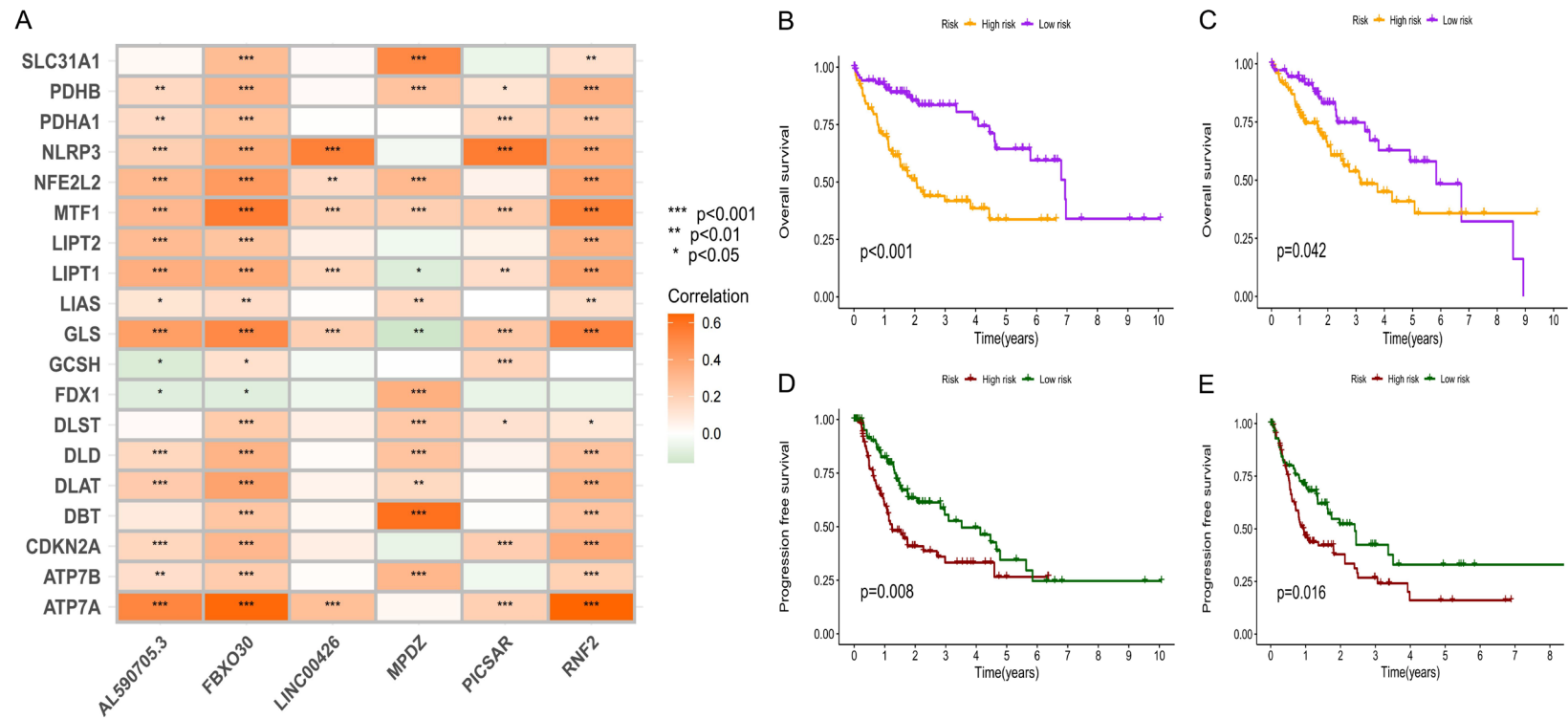


Figure 3. Validation of the prognostic model for HCC. (A) Heatmap of the correlation analysis between the LncRNAs/mRNAs in the prognostic model and cuproptosis-related genes. Survival analysis of OS and PFS in HCC patients between the high- and low-risk in the training group (B, C) and the testing group (D, E) using the prognostic model. (* $P < 0.05$, ** $P < 0.01$, *** $P < 0.001$).

Cuproptosis-related signatures predicted prognosis of HCC

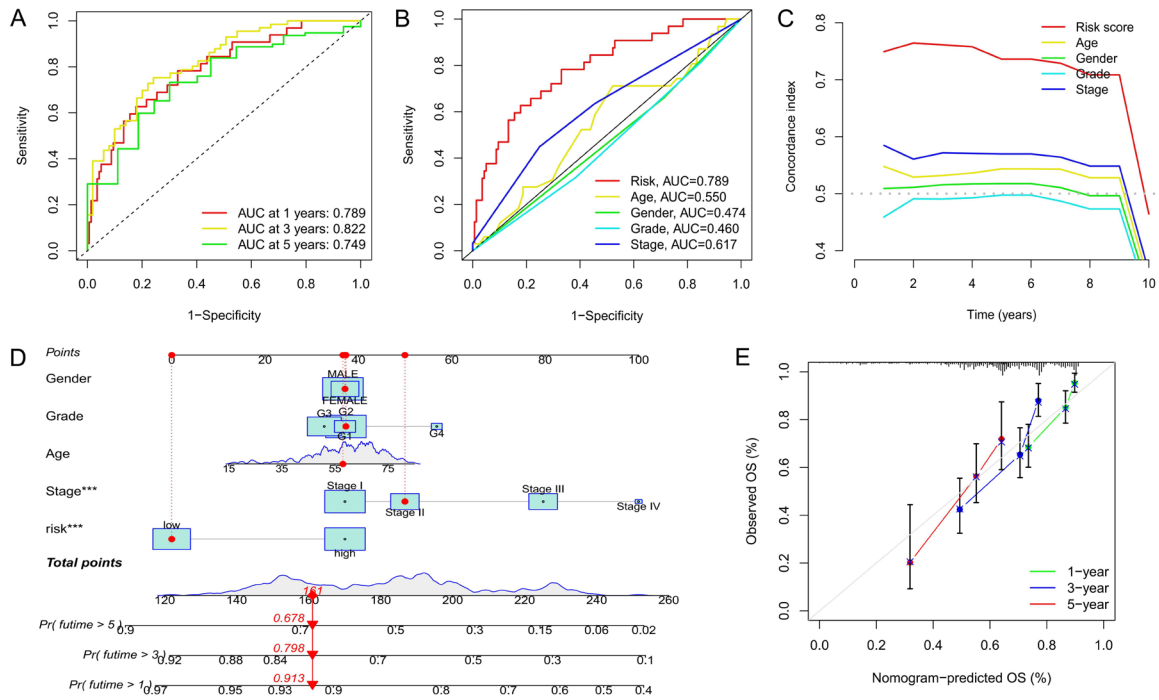


Figure 4. Validation of the clinical characteristics of prognostic models and construction of nomogram. A. ROC curves for predicting 1-, 3-, and 5-year OS in HCC. B. ROC curves for predicting OS with risk score and clinical characteristics. C. Concordant index analysis of risk score and clinical characteristics to predict OS. D. Nomogram for predicting 1-, 3-, and 5-year OS in HCC. E. Calibration curve to verify the accuracy of nomogram prediction. (* $P < 0.05$, ** $P < 0.01$, *** $P < 0.001$).

cell co-inhibition”, “Cytolytic activity”, “APC co-inhibition”, “Type I IFN Response”, “Parainflammation”, “Check point”, “T cell co stimulation”, “Inflammation promoting”, and “HLA” immune pathways. All of these immune functional pathways were more active in the low-risk group (Figure 5A). Moreover, we used TIDE score to analyze the immune escape potential to evaluate the effect of immunotherapy and found that there was a greater potential for immune escape in the low-risk group, suggesting the possibility of poor response to immunotherapy (Figure 5B). Furthermore, the analysis of 22 types of immune cells showed that “Macrophages M0” infiltration was significantly different between the high- and low-risk groups and was upregulated in the high-risk group (Figure 5C).

Importantly, we conducted drug sensitivity analysis for the high- and low-risk groups to identify potential sensitive drugs that could be beneficial to HCC patients. We found three drugs, XAV939, JNJ-26854165 and ATRA, were more sensitive in the the low-risk group

(Supplementary Figure 6A-C), while Paclitaxel, JW-7-52-1, Thapsigargin, GW843682X, Gemcitabine, FR-180204, Epothilone, Doxorubicin, BMS-509744, BIX02189, BI-2536, and S-Trityl-L-cysteine were more sensitive in the high-risk group (Supplementary Figure 6D-O). The specific mechanism of action and targeted pathway of these drugs were predicted in Genomics of Drug Sensitivity in Cancer (<https://www.cancerrxgene.org/>). The correlation between the IC50 value of these 15 drugs and the risk score of patients were presented by scatter plots (Supplementary Figure 7A-O). We listed scatter plots with absolute values of $R > 0.40$ [13].

Discussion

HCC is increasingly prevalent worldwide, especially in China, accounting for about 50% of the total global cases, where HCC is the second most malignant cancer after lung cancer, mainly caused by hepatitis B cirrhosis [15]. Due to the lack of clinical symptoms on the early stage of HCC, most patients have developed middle or late stage of HCC at the time of diagnosis

Cuproptosis-related signatures predicted prognosis of HCC

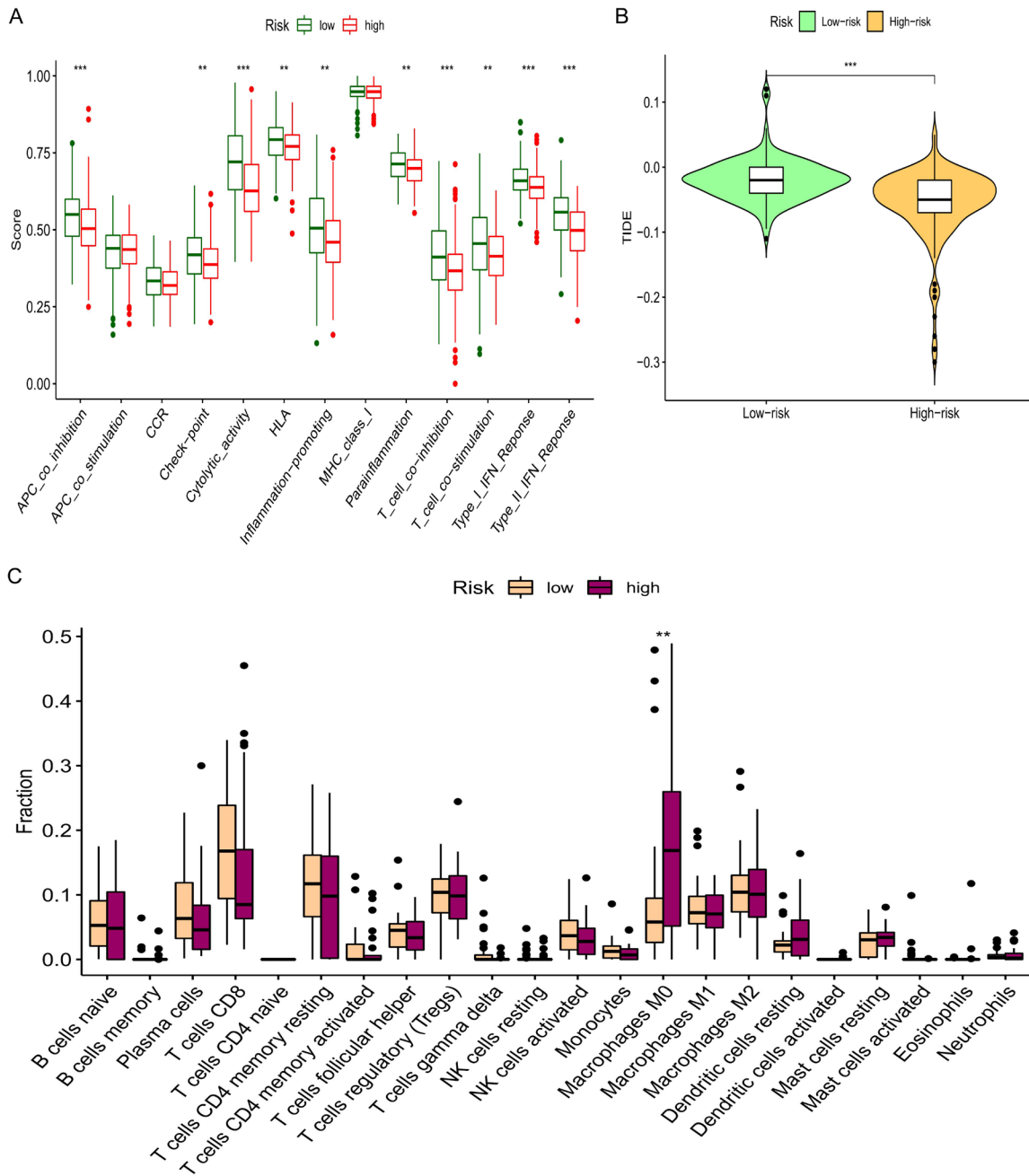


Figure 5. Immune function and immune escape. A. Analysis of the activity of immune function pathways in the high- and low-risk groups in prognostic model. B. Analysis of immune escape in the high- and low-risk groups. The higher the TIDE score, the greater the immune escape potential, and the worse the immunotherapy effect. C. Analysis of immune cell infiltration in the high- and low-risk groups in prognostic model. (* $P < 0.05$, ** $P < 0.01$, *** $P < 0.001$).

and, therefore, have missed the best opportunity for surgical treatment. In recent years, the recurrence rate after postoperative resection is also increased [16]. In addition, the traditional chemotherapy method has not achieved satisfactory therapeutic effect. However, the rapid development of targeted therapy and immunotherapy has brought new hope to HCC patients. Currently, three targeted drugs (sorafenib, rego-

rafenib, and Lenvatinib) have been approved by the US Food and Drug Administration (FDA) for the treatment of advanced HCC [17]. Meanwhile, based on the remarkable results in phase II clinical trials, the anti-PD-1 monoclonal antibody Nivolumab is granted accelerated approval by FDA to treat advanced HCC [18]. Although these drugs have brought new treatment options to advanced HCC, the low objective

response rate and unavoidable acquired drug resistance due to the heterogeneity of HCC are clinical challenges when using these therapies [19-22]. While the survival rates for most cancers worldwide are improving, the survival rate for liver cancer remains unchanged, especially in China [23]. Therefore, it is crucial to identify new biomarkers for the early diagnosis and effective treatment strategies for HCC. In this study, we focused on the cuproptosis-related genes and combined the gene transcriptome data and the clinical characteristics of HCC to construct a comprehensive cuproptosis-related signature-based prognostic model, which might provide a new insight for HCC treatment.

In our study, 17 Cuproptosis-related genes and 3449 lncRNAs/mRNAs co-expressed in HCC were extracted from the transcriptome data of 374 TCGA samples. We then combined the clinical data of 370 TCGA samples with 3 mRNAs (FBXO30, RNF2, MPDZ) and 3 lncRNAs (AL590705.3, PICSAR, LINC00426) identified by Cox regression and LASSO regression analyses to construct the prognostic model. FBXO30 (F-box protein 30), a member of the F-box protein family, is an orphan molecule without known substrate or function [24]. In the animal studies by Liu et al. [24], FBXO30 was demonstrated to be an E3 ligase that specifically ubiquitinated and regulated mitotic spindle kinesin EG5 levels in embryonic fibroblasts and mammary epithelial cells. Since EG5 expression has been shown to be elevated in cancer patients and is correlated with poor prognosis [25], Liu et al. speculated that the elevated EG5 protein levels were associated with reduced FBXO30 levels in cancers. However, paradoxically, other studies have shown that FBXO30 expression is upregulated in nasopharyngeal cancers [26], which was consistent with our findings in this study that high expression of FBXO30 was associated with poor prognosis. Nevertheless, the role of FBXO30 in HCC needs to be further investigated. On the other hand, RNF2 (ring finger protein 2) is an E3 ubiquitin ligase of the ring finger protein family. The dysregulation of RNF2 expression in cancers has been widely reported, and the up-regulation of RNF2 was involved in the progression of breast cancer [27, 28], lung cancer [29], colorectal cancer [30], prostate cancer [31], gastric cancer [32], and HCC [33], as well as was associated with poor prognosis.

Similarly, our prognostic model also confirmed that RNF2 expression was upregulated in the high-risk group, and the patients with high RNF2 expression had worse survival outcomes. As for MPDZ (multiple PSD95-Discs large-ZO1) domain protein, it is a large adaptor protein involved in the binding to the C-terminus of other proteins. For example, MPDZ binds to serotonin receptors or G protein-coupled receptors to function in hydrocephalus, alcohol addiction, and neurological disorders [34-36]. Recently, in the study of Liu et al. [37], MPDZ was proposed as a tumor suppressor gene as MPDZ overexpression significantly inhibited the growth, migration, and invasion of lung cancer cells. In addition, low expression or deletion of MPDZ has been suggested to be significantly associated with poor prognosis of renal clear cell carcinoma [38]; however, the role of MPDZ in HCC has not been reported. In our prognostic model, the expression of MPDZ was up-regulated in the low-risk group, and the high expression of MPDZ predicted better survival, suggesting the potential tumor suppressing function of MPDZ in HCC, which needs to be further experimentally validated.

Currently, no information about lncRNA AL590705.3 has been reported, and there are only few reports about lncRNA PICSAR (P38 inhibited cutaneous squamous cell carcinoma associated lncRNA), also known as LINC00162. The function and its underlying mechanism of PICSAR in cancer was first reported in cutaneous squamous cell carcinoma [39] (cSCC), where upregulation of PICSAR promoted the progression of cSCC and was involved in cisplatin resistance [39-41]. More importantly, PICSAR has been reported to play a cancer-promoting role by targeting miR-588 in HCC [42]. With regard to LINC00426, also known as ENSG00000238121, it was reported to accelerate lung adenocarcinoma progression by regulating miR-455-5p and promote doxorubicin resistance by secreting miR-4319 in osteosarcoma [43, 44]. However, some studies showed that LINC00426 was downregulated in colorectal cancer and non-small cell lung cancer [45]. In addition, a series of bioinformatics analyses indicated that LINC00426 could be used as a prognostic marker for cervical cancer, renal clear cell carcinoma, and HCC [46-48]. Importantly, Zhu et al. reported the down-regulation of LINC00426 expression in HCC

patients, which was consistent with our findings [47].

In our prognostic model, stage and risk score were independent prognostic factors for HCC. The later the cancer stage, the higher the risk score, and the worse the prognosis. Based on the gene expression levels of the selected panels, we generated survival estimation nomograms. This nomogram could be clinically useful as each patient could get the unique nomogram through R software, which is almost free, portable, and intuitive for clinical application. More importantly, we explored the application of our predictive model in immunotherapy. Since there are no large-scale transcriptome data for HCC immunotherapy, we used the immune dysfunction and exclusion score in TIDE database to analyze the potential of immune escape and predict the effectiveness of immunotherapy. Our study found that HCC patients in the high-risk group might respond better to immunotherapy. Lastly, we also screened potential sensitive drugs to provide a reference for future drug selection.

Although our cuproptosis-related lncRNAs/mRNAs prognostic model yielded some important findings, it had some limitations. Our studies investigated the influence of immune infiltration and gene mutation on the progression of HCC; however, other factors such as epigenetic modifications are important in the pathology of the disease. An analysis combining these factors will provide more insights in understanding the development of HCC. In future studies, we will also continue to refine the data and risk models to ensure more robust prediction.

Conclusion

In summary, our study was the first to reveal the relationship between cuproptosis-related lncRNAs/mRNAs signatures and the prognosis of patients with HCC. We constructed a prognostic model to assess the immunotherapy efficacy, screen for potentially sensitive drugs, and predict disease prognosis. These information could be used in target selection and individualized immunotherapy of HCC.

Acknowledgements

This research was supported by the National Natural Science Foundation of China (No.

81372487) and the Natural Science Foundation of Hefei (No. 2022034). The authors would like to thank Veritas EdSci (www.veritasedsci.com) for its linguistic assistance during the preparation of this manuscript. Also, the authors thank the TCGA and TIDE databases for providing valuable data sets.

Disclosure of conflict of interest

None.

Address correspondence to: Huaidong Cheng, Department of Oncology, The Second Affiliated Hospital of Anhui Medical University, No. 678 Furong Road, Hefei 230601, Anhui, China. Tel: +86-0551-63869542; Fax: +86-0551-63869400; ORCID: 0000-0001-6422-1257; E-mail: chd1975ay@126.com

References

- [1] Sung H, Ferlay J, Siegel RL, Laversanne M, Soerjomataram I, Jemal A and Bray F. Global cancer statistics 2020: GLOBOCAN estimates of incidence and mortality worldwide for 36 cancers in 185 countries. *CA Cancer J Clin* 2021; 71: 209-249.
- [2] Chen S, Cao Q, Wen W and Wang H. Targeted therapy for hepatocellular carcinoma: challenges and opportunities. *Cancer Lett* 2019; 460: 1-9.
- [3] Llovet JM, Zucman-Rossi J, Pikarsky E, Sangro B, Schwartz M, Sherman M and Gores G. Hepatocellular carcinoma. *Nat Rev Dis Primers* 2016; 2: 16018.
- [4] Lin S, Hoffmann K and Schemmer P. Treatment of hepatocellular carcinoma: a systematic review. *Liver Cancer* 2012; 1: 144-158.
- [5] Tsvetkov P, Coy S, Petrova B, Dreishpoon M, Verma A, Abdusamad M, Rossen J, Joesch-Cohen L, Humeidi R, Spangler RD, Eaton JK, Frenkel E, Kocak M, Corsello SM, Lutsenko S, Kanarek N, Santagata S and Golub TR. Copper induces cell death by targeting lipoylated TCA cycle proteins. *Science* 2022; 375: 1254-1261.
- [6] Brady DC, Crowe MS, Greenberg DN and Counter CM. Copper chelation inhibits BRAF(V600E)-driven melanomagenesis and counters resistance to BRAF(V600E) and MEK1/2 inhibitors. *Cancer Res* 2017; 77: 6240-6252.
- [7] Gromadzka G, Tarnacka B, Flaga A and Adamczyk A. Copper dyshomeostasis in neurodegenerative diseases-therapeutic implications. *Int J Mol Sci* 2020; 21: 9259.
- [8] Kardos J, Héja L, Simon Á, Jablonkai I, Kovács R and Jemnitz K. Copper signalling: causes

Cuproptosis-related signatures predicted prognosis of HCC

- and consequences. *Cell Commun Signal* 2018; 16: 71.
- [9] Kurutas EB. The importance of antioxidants which play the role in cellular response against oxidative/nitrosative stress: current state. *Nutr J* 2016; 15: 71.
- [10] Niedzielska E, Smaga I, Gawlik M, Moniczewska A, Stankowicz P, Pera J and Filip M. Oxidative stress in neurodegenerative diseases. *Mol Neurobiol* 2016; 53: 4094-4125.
- [11] Horn N, Møller LB, Nurchi VM and Aaseth J. Chelating principles in Menkes and Wilson diseases: choosing the right compounds in the right combinations at the right time. *J Inorg Biochem* 2019; 190: 98-112.
- [12] O'Day SJ, Eggermont AM, Chiarion-Sileni V, Kefford R, Grob JJ, Mortier L, Robert C, Schachter J, Testori A, Mackiewicz J, Friedlander P, Garbe C, Ugurel S, Collichio F, Guo W, Lufkin J, Bahcall S, Vukovic V and Hauschild A. Final results of phase III SYMMETRY study: randomized, double-blind trial of elesclomol plus paclitaxel versus paclitaxel alone as treatment for chemotherapy-naïve patients with advanced melanoma. *J Clin Oncol* 2013; 31: 1211-1218.
- [13] Schober P, Boer C and Schwarte LA. Correlation coefficients: appropriate use and interpretation. *Anesth Analg* 2018; 126: 1763-1768.
- [14] Chen W, Zheng R, Baade PD, Zhang S, Zeng H, Bray F, Jemal A, Yu XQ and He J. Cancer statistics in China, 2015. *CA Cancer J Clin* 2016; 66: 115-132.
- [15] Sperber AD, Bangdiwala SI, Drossman DA, Ghoshal UC, Simren M, Tack J, Whitehead WE, Dumitrascu DL, Fang X, Fukudo S, Kellow J, Okeke E, Quigley EMM, Schmulson M, Whorwell P, Archampong T, Adibi P, Andresen V, Benninga MA, Bonaz B, Bor S, Fernandez LB, Choi SC, Corazzari ES, Francisconi C, Hani A, Lazebnik L, Lee YY, Mulak A, Rahman MM, Santos J, Setshedi M, Syam AF, Vanner S, Wong RK, Lopez-Colombo A, Costa V, Dickman R, Kanazawa M, Keshteli AH, Khatun R, Maleki I, Poitras P, Pratap N, Stefanyuk O, Thomson S, Zeevenhooven J and Palsson OS. Worldwide prevalence and burden of functional gastrointestinal disorders, results of rome foundation global study. *Gastroenterology* 2021; 160: 99-114, e113.
- [16] Liu D and Song T. Changes in and challenges regarding the surgical treatment of hepatocellular carcinoma in China. *Biosci Trends* 2021; 15: 142-147.
- [17] Dhanasekaran R, Nault JC, Roberts LR and Zucman-Rossi J. Genomic medicine and implications for hepatocellular carcinoma prevention and therapy. *Gastroenterology* 2019; 156: 492-509.
- [18] El-Khoueiry AB, Sangro B, Yau T, Crocenzi TS, Kudo M, Hsu C, Kim TY, Choo SP, Trojan J, Welling TH Rd, Meyer T, Kang YK, Yeo W, Chopra A, Anderson J, Dela Cruz C, Lang L, Neely J, Tang H, Dastani HB and Melero I. Nivolumab in patients with advanced hepatocellular carcinoma (CheckMate 040): an open-label, non-comparative, phase 1/2 dose escalation and expansion trial. *Lancet* 2017; 389: 2492-2502.
- [19] Demetri GD, Reichardt P, Kang YK, Blay JY, Rutkowski P, Gelderblom H, Hohenberger P, Leahy M, von Mehren M, Joensuu H, Badalamenti G, Blackstein M, Le Cesne A, Schöffski P, Maki RG, Bauer S, Nguyen BB, Xu J, Nishida T, Chung J, Kappeler C, Kuss I, Laurent D and Casali PG. Efficacy and safety of regorafenib for advanced gastrointestinal stromal tumours after failure of imatinib and sunitinib (GRID): an international, multicentre, randomised, placebo-controlled, phase 3 trial. *Lancet* 2013; 381: 295-302.
- [20] Grothey A, Van Cutsem E, Sobrero A, Siena S, Falcone A, Ychou M, Humblet Y, Bouché O, Mineur L, Barone C, Adenis A, Tabernero J, Yoshino T, Lenz HJ, Goldberg RM, Sargent DJ, Cichon F, Cupit L, Wagner A and Laurent D. Regorafenib monotherapy for previously treated metastatic colorectal cancer (CORRECT): an international, multicentre, randomised, placebo-controlled, phase 3 trial. *Lancet* 2013; 381: 303-312.
- [21] Ikeda K, Kudo M, Kawazoe S, Osaki Y, Ikeda M, Okusaka T, Tamai T, Suzuki T, Hisai T, Hayato S, Okita K and Kumada H. Phase 2 study of lenvatinib in patients with advanced hepatocellular carcinoma. *J Gastroenterol* 2017; 52: 512-519.
- [22] Fu J and Wang H. Precision diagnosis and treatment of liver cancer in China. *Cancer Lett* 2018; 412: 283-288.
- [23] Allemani C, Matsuda T, Di Carlo V, Harewood R, Matz M, Nikšić M, Bonaventure A, Valkov M, Johnson CJ, Estève J, Ogunbiyi OJ, Azevedo E Silva G, Chen WQ, Eser S, Engholm G, Stiller CA, Monnereau A, Woods RR, Visser O, Lim GH, Aitken J, Weir HK and Coleman MP. Global surveillance of trends in cancer survival 2000-14 (CONCORD-3): analysis of individual records for 37513025 patients diagnosed with one of 18 cancers from 322 population-based registries in 71 countries. *Lancet* 2018; 391: 1023-1075.
- [24] Liu Y, Wang Y, Du Z, Yan X, Zheng P and Liu Y. Fbxo30 regulates mammopoiesis by targeting the bipolar mitotic kinesin Eg5. *Cell Rep* 2016; 15: 1111-1122.
- [25] Ding S, Xing N, Lu J, Zhang H, Nishizawa K, Liu S, Yuan X, Qin Y, Liu Y, Ogawa O and Nishiyama

Cuproptosis-related signatures predicted prognosis of HCC

- H. Overexpression of Eg5 predicts unfavorable prognosis in non-muscle invasive bladder urothelial carcinoma. *Int J Urol* 2011; 18: 432-438.
- [26] Bjerre MT, Strand SH, Nørgaard M, Kristensen H, Rasmussen AK, Mortensen MM, Fredsøe J, Mouritzen P, Ulhøi B, Ørntoft T, Borre M and Sørensen KD. Aberrant DOCK2, GRASP, HIF3A and PKFP hypermethylation has potential as a prognostic biomarker for prostate cancer. *Int J Mol Sci* 2019; 20: 1173.
- [27] Wu J, Wang H, Li Q, Guo QY, Tao SQ, Shen YX and Wu ZS. The oncogenic impact of RNF2 on cell proliferation, invasion and migration through EMT on mammary carcinoma. *Pathol Res Pract* 2019; 215: 152523.
- [28] Chan HL, Beckedorff F, Zhang Y, Garcia-Huidobro J, Jiang H, Colaprico A, Bilbao D, Figueroa ME, LaCava J, Shiekhhattar R and Morey L. Polycomb complexes associate with enhancers and promote oncogenic transcriptional programs in cancer through multiple mechanisms. *Nat Commun* 2018; 9: 3377.
- [29] Yang J, Yu F, Guan J, Wang T, Liu C, Wang Y, Liu G and Zhu S. Knockdown of RNF2 enhances the radiosensitivity of squamous cell carcinoma in lung. *Biochem Cell Biol* 2019; 97: 589-599.
- [30] Wang J, Ouyang X, Zhou Z, Mao S, Niu X, Li H, Xu W, Song Y, Cao J and Lai B. RNF2 promotes the progression of colon cancer by regulating ubiquitination and degradation of IRF4. *Biochim Biophys Acta Mol Cell Res* 2022; 1869: 119162.
- [31] Wei M, Jiao D, Han D, Wu J, Wei F, Zheng G, Guo Z, Xi W, Yang F, Xie P, Zhang L, Yang AG, Wang H, Qin W and Wen W. Knockdown of RNF2 induces cell cycle arrest and apoptosis in prostate cancer cells through the upregulation of TXNIP. *Oncotarget* 2017; 8: 5323-5338.
- [32] Yue F, Peng K, Zhang L and Zhang J. Circ_0004104 accelerates the progression of gastric cancer by regulating the miR-539-3p/RNF2 axis. *Dig Dis Sci* 2021; 66: 4290-4301.
- [33] Qu C and Qu Y. Down-regulation of salt-inducible kinase 1 (SIK1) is mediated by RNF2 in hepatocarcinogenesis. *Oncotarget* 2017; 8: 3144-3155.
- [34] Kruse LC, Walter NA and Buck KJ. Mpdz expression in the caudolateral substantia nigra pars reticulata is crucially involved in alcohol withdrawal. *Genes Brain Behav* 2014; 13: 769-776.
- [35] Yang J, Simonneau C, Kilker R, Oakley L, Byrne MD, Nichtova Z, Stefanescu I, Pardeep-Kumar F, Tripathi S, Londin E, Saugier-Veber P, Willard B, Thakur M, Pickup S, Ishikawa H, Schroten H, Smeyne R and Horowitz A. Murine MPDZ-linked hydrocephalus is caused by hyperpermeability of the choroid plexus. *EMBO Mol Med* 2019; 11: e9540.
- [36] Guillaume JL, Daulat AM, Maurice P, Levoye A, Migaud M, Brydon L, Malpoux B, Borg-Capra C and Jockers R. The PDZ protein mupp1 promotes Gi coupling and signaling of the Mt1 melatonin receptor. *J Biol Chem* 2008; 283: 16762-16771.
- [37] Liu W, Huang Y, Wang D, Han F, Chen H, Chen J, Jiang X, Cao J and Liu J. MPDZ as a novel epigenetic silenced tumor suppressor inhibits growth and progression of lung cancer through the Hippo-YAP pathway. *Oncogene* 2021; 40: 4468-4485.
- [38] Huang YS, Liu WB, Han F, Yang JT, Hao XL, Chen HQ, Jiang X, Yin L, Ao L, Cui ZH, Cao J and Liu JY. Copy number variations and expression of MPDZ are prognostic biomarkers for clear cell renal cell carcinoma. *Oncotarget* 2017; 8: 78713-78725.
- [39] Piipponen M, Nissinen L, Farshchian M, Riihilä P, Kivisaari A, Kallajoki M, Peltonen J, Peltonen S and Kähäri VM. Long noncoding RNA PICSAR promotes growth of cutaneous squamous cell carcinoma by regulating ERK1/2 activity. *J Invest Dermatol* 2016; 136: 1701-1710.
- [40] Lu X, Gan Q, Gan C, Zheng Y, Cai B, Li X, Li D and Yin G. Long non-coding RNA PICSAR knockdown inhibits the progression of cutaneous squamous cell carcinoma by regulating miR-125b/YAP1 axis. *Life Sci* 2021; 274: 118303.
- [41] Wang D, Zhou X, Yin J and Zhou Y. Lnc-PICSAR contributes to cisplatin resistance by miR-485-5p/REV3L axis in cutaneous squamous cell carcinoma. *Open Life Sci* 2020; 15: 488-500.
- [42] Liu Z, Mo H, Sun L, Wang L, Chen T, Yao B, Liu R, Niu Y, Tu K, Xu Q and Yang N. Long noncoding RNA PICSAR/miR-588/EIF6 axis regulates tumorigenesis of hepatocellular carcinoma by activating PI3K/AKT/mTOR signaling pathway. *Cancer Sci* 2020; 111: 4118-4128.
- [43] Li H, Mu Q, Zhang G, Shen Z, Zhang Y, Bai J, Zhang L, Zhou D, Zheng Q, Shi L, Su W, Yin C and Zhang B. Linc00426 accelerates lung adenocarcinoma progression by regulating miR-455-5p as a molecular sponge. *Cell Death Dis* 2020; 11: 1051.
- [44] Wang L, Luo Y, Zheng Y, Zheng L, Lin W, Chen Z, Wu S, Chen J and Xie Y. Long non-coding RNA LINC00426 contributes to doxorubicin resistance by sponging miR-4319 in osteosarcoma. *Biol Direct* 2020; 15: 11.
- [45] Best MG, Sol N, Kooi I, Tannous J, Westerman BA, Rustenburg F, Schellen P, Verschueren H, Post E, Koster J, Ylstra B, Ameziane N, Dorsman J, Smit EF, Verheul HM, Noske DP, Reijneveld JC, Nilsson RJA, Tannous BA, Wesseling P and Wurdinger T. RNA-seq of tumor-

Cuproptosis-related signatures predicted prognosis of HCC

- educated platelets enables blood-based pan-cancer, multiclass, and molecular pathway cancer diagnostics. *Cancer Cell* 2015; 28: 666-676.
- [46] Lv X, Liu L, Li P, Yuan Y, Peng M, Jin H and Qin D. Constructing a novel signature based on immune-related lncRNA to improve prognosis prediction of cervical squamous cell carcinoma patients. *Reprod Sci* 2022; 29: 800-815.
- [47] Zhu R, Guo W, Xu XJ and Zhu L. An integrating immune-related signature to improve prognosis of hepatocellular carcinoma. *Comput Math Methods Med* 2020; 2020: 8872329.
- [48] Xiang Z, Shen E, Li M, Hu D, Zhang Z and Yu S. Potential prognostic biomarkers related to immunity in clear cell renal cell carcinoma using bioinformatic strategy. *Bioengineered* 2021; 12: 1773-1790.

Cuproptosis-related signatures predicted prognosis of HCC

Supplementary Table 1. TCGA database retrieval strategy

Data type	Retrieval strategy
Transcriptome data	cases disease type in ["adenomas and adenocarcinomas"] AND cases primary site in ["liver and intrahepatic bile ducts"] AND cases project program name in ["TCGA"] AND cases project identification (ID) in ["TCGA-LIHC"] AND files access in ["open"] and files analysis workflow type in ["STAR-Counts"] AND files data category in ["transcriptome profiling"] AND files data type in ["Gene Expression Quantification"]
Clinical data	cases disease type in ["adenomas and adenocarcinomas"] AND cases primary site in ["liver and intrahepatic bile ducts"] and cases project program name in ["TCGA"] AND cases project ID in ["TCGA-LIHC"] AND files access in ["open"] and files data category in ["clinical"] AND files data format in ["bcr xml"] AND files data type in ["Clinical Supplement"]
Gene mutation data	cases primary site in ["liver and intrahepatic bile ducts"] AND cases project program name in ["TCGA"] AND cases project ID in ["TCGA-LIHC"] AND files access in ["open"] AND files analysis workflow type in ["Aliquot Ensemble Somatic Variant Merging and Masking"] AND files data category in ["simple nucleotide variation"] AND files data format in ["maf"] AND files data type in ["Masked Somatic Mutation"]

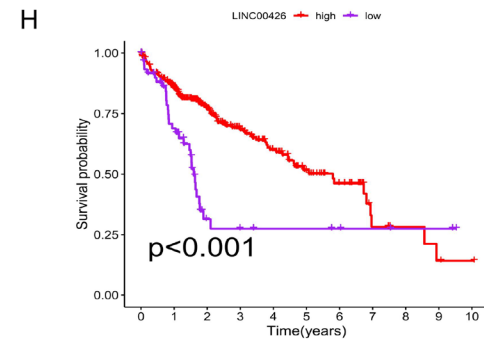
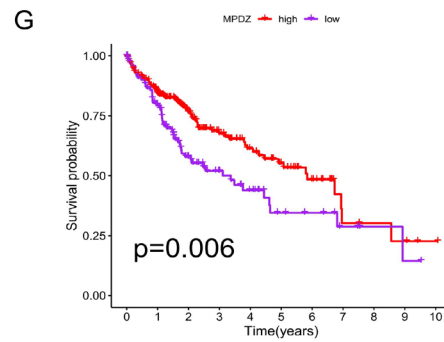
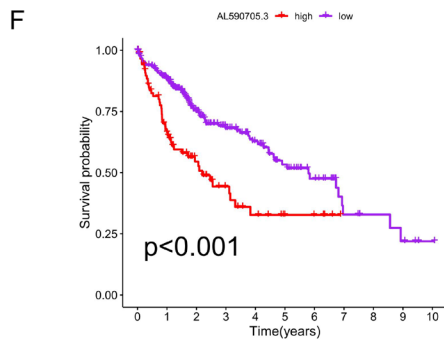
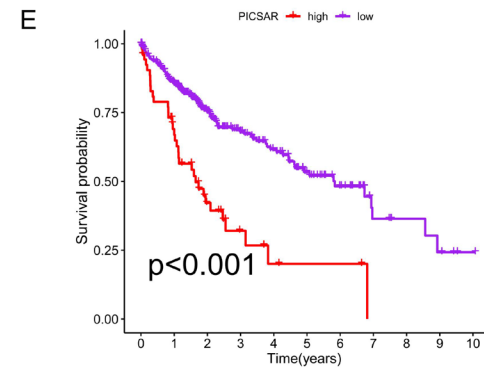
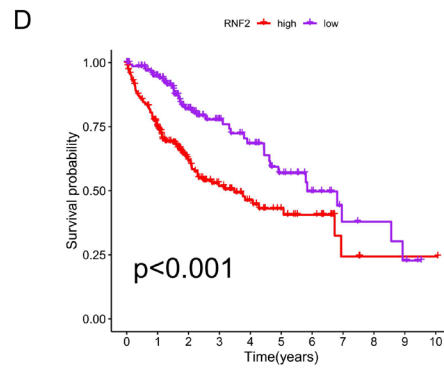
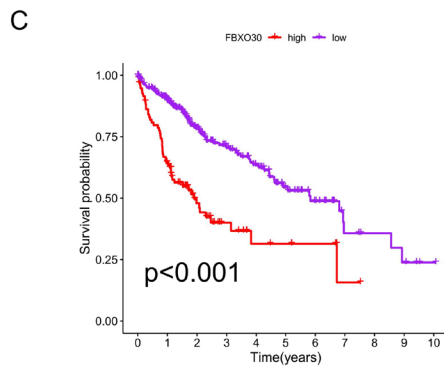
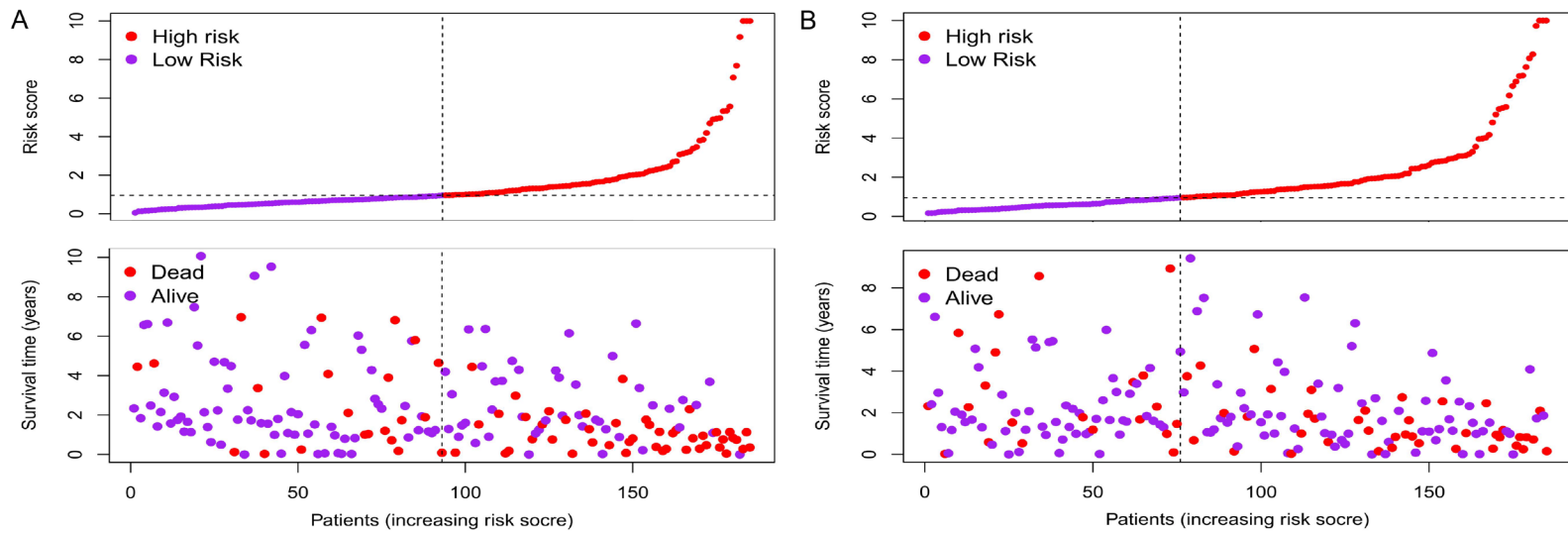
Supplementary Table 2. Cuproptosis-related genes

Gens	Full name
NFE2L2	nuclear factor erythroid 2-related factor 2
NLRP3	Nod-like receptor pyrin domain containing 3
ATP7B	adenosine triphosphatase copper transporting beta
ATP7A	adenosine triphosphatase copper transporting alpha
SLC31A1	solute carrier family 31 member 1
FDX1	ferredoxin 1
LIAS	lipoic acid synthase
LIPT1	lipoyl(octanoyl) transferase 1
LIPT2	lipoyl(octanoyl) transferase 2
DLD	dihydrolipoamide dehydrogenase
DLAT	dihydrolipoyllysine acetyltransferase
PDHA1	pyruvate dehydrogenase alpha 1
PDHB	pyruvate dehydrogenase beta
MTF1	metal-regulatory transcription factor-1
GLS	glutaminase
CDKN2A	cyclin-dependent kinase inhibitor alpha
DBT	dihydrolipoamide branched chain transacylase
GCSH	glycine cleavage system protein H
DLST	dihydrolipoamide S-succinyltransferase

Supplementary Table 3. Information of the qPCR primer sequences

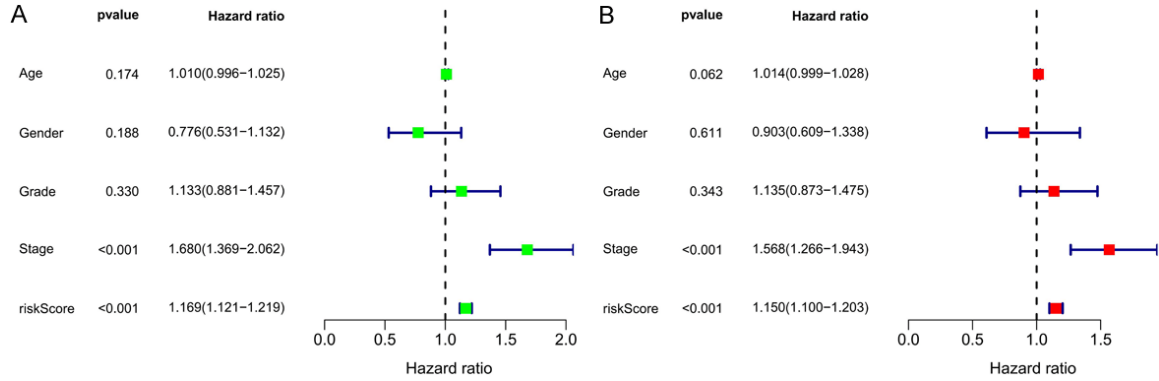
	Forward (5' to 3')	Reverse (5' to 3')
GAPDH	AAGGTGAAGGTCGGAGTCAAC	GGGGTCATTGATGGCAACAATA
FBXO30	GGGGACGTGAAGAATGTGGA	ATCAGCCATGCGGCTATCAG
RNF2	GCCAGGATCAACAAGCACAATAA	CTGCTTCTGATTGCTATGTGTG
MPDZ	GTTTAGGAGCGAGTTAAATTC	CTAAACTACCGTAACGCCTACG
PICSA	ACTGCCTGGACTTCAAGAGG	CCTCTGGGTAGGGTGTGG
LINC00426	CAAGAAGACAGGGACAAGC	ACTGAGTACCCAGCCAAAG
AL590705.3	ATTTAATTGTGGTCTGCCAAGGA	CCAAGTGGTCTCTCCAACC

Cuproptosis-related signatures predicted prognosis of HCC

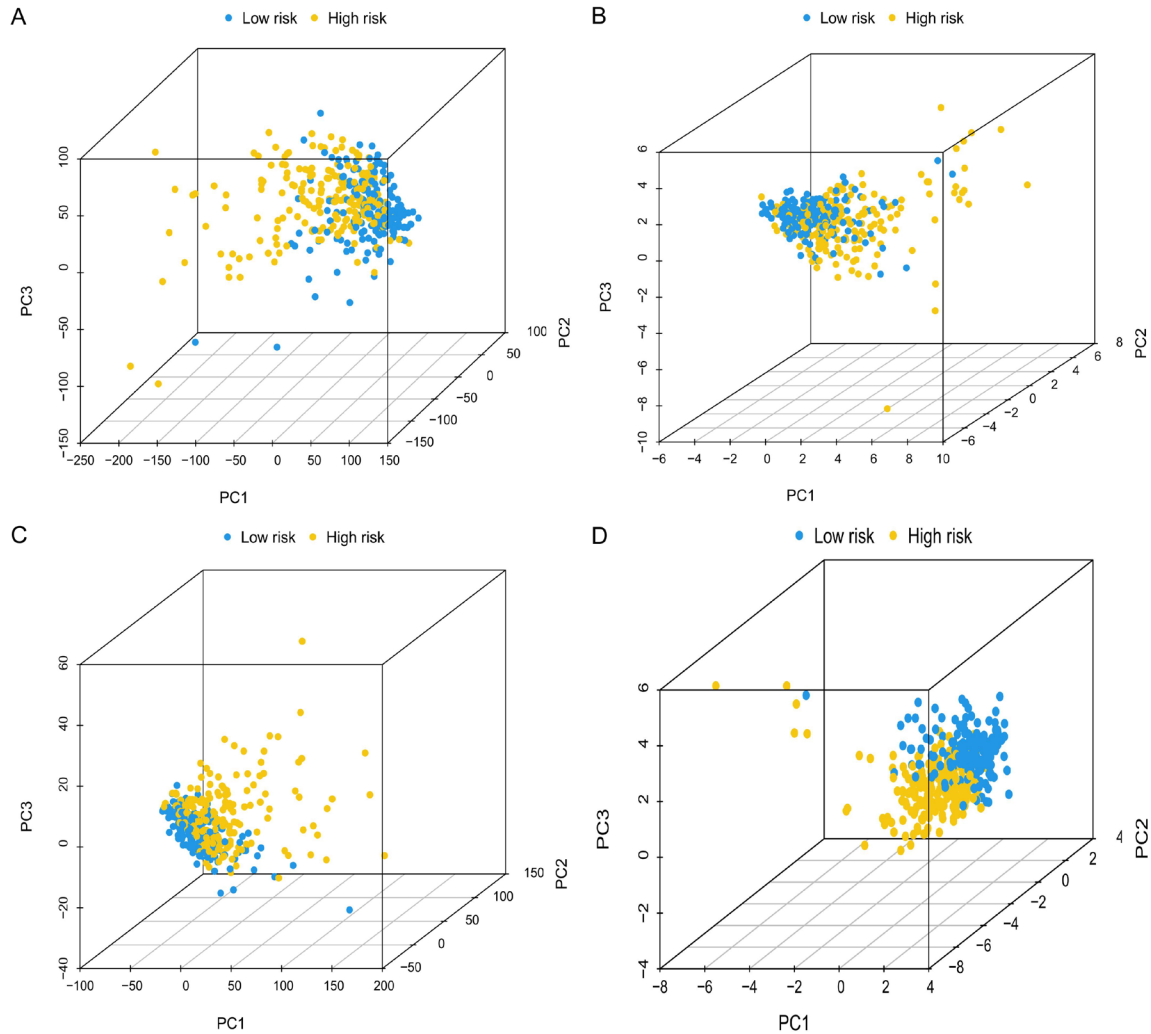


Cuproptosis-related signatures predicted prognosis of HCC

Supplementary Figure 1. Risk analysis of prognostic models and K-M analysis of signatures. (A, B) HCC patients in training group and testing group were divided into high- group and low-risk group according to the median value of risk score. With the increase of risk score, the number of deaths increased correspondingly, and the survival prognosis of patients with low-risk was better. K-M analysis showed that high expression of (C) FBXO30, (D) RNF2, (E) PICSAR, (F) AL590705.3 and low expression of (G) MPDZ and (H) LINC00426 in HCC were associated with poor OS.

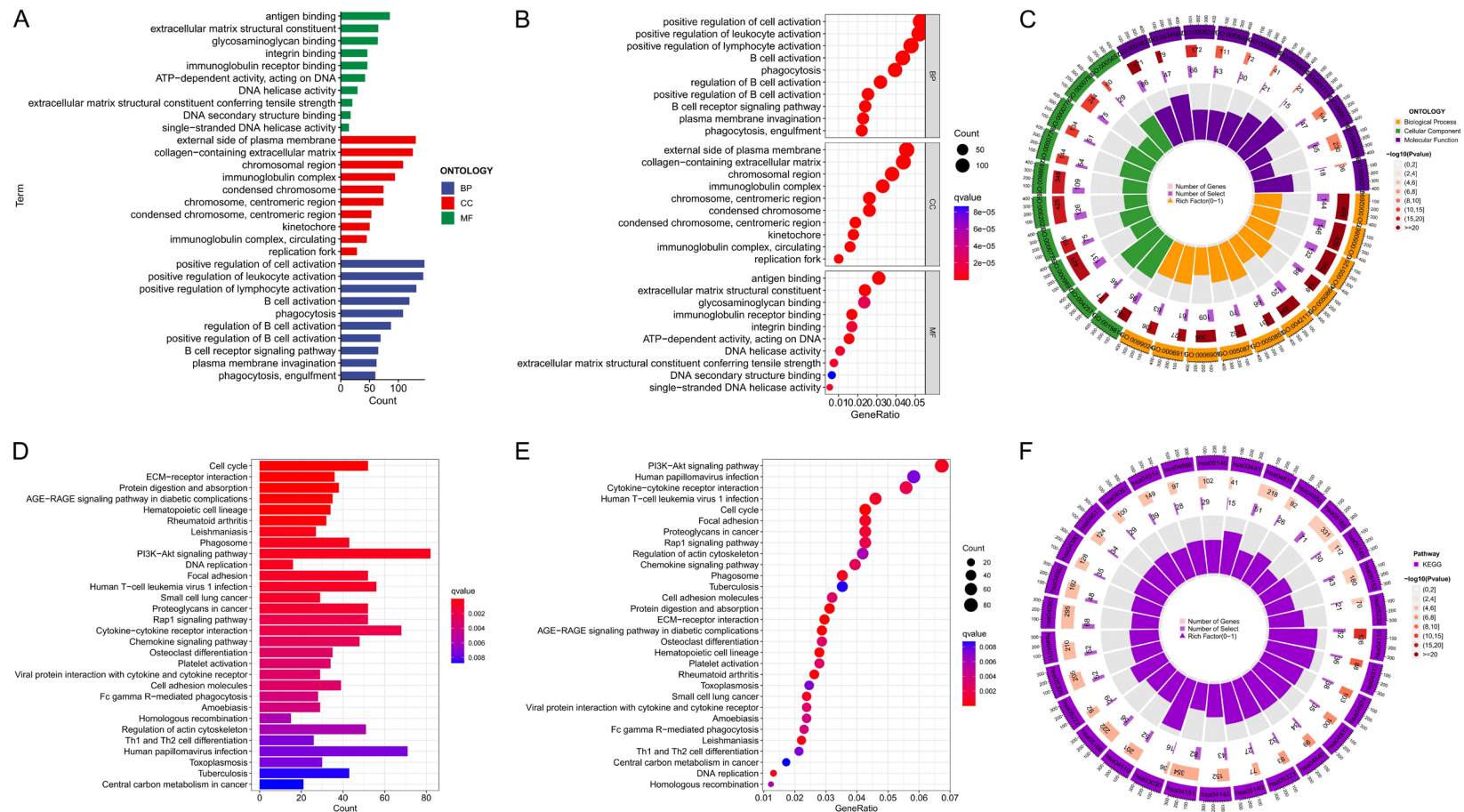


Supplementary Figure 2. Analysis of independent prognostic factors. A. Univariate analysis showed that stage and risk score were correlated with patient's prognosis. B. Multivariate analysis confirmed that stage and score were independent prognostic factors for predicting the OS of patients with HCC.



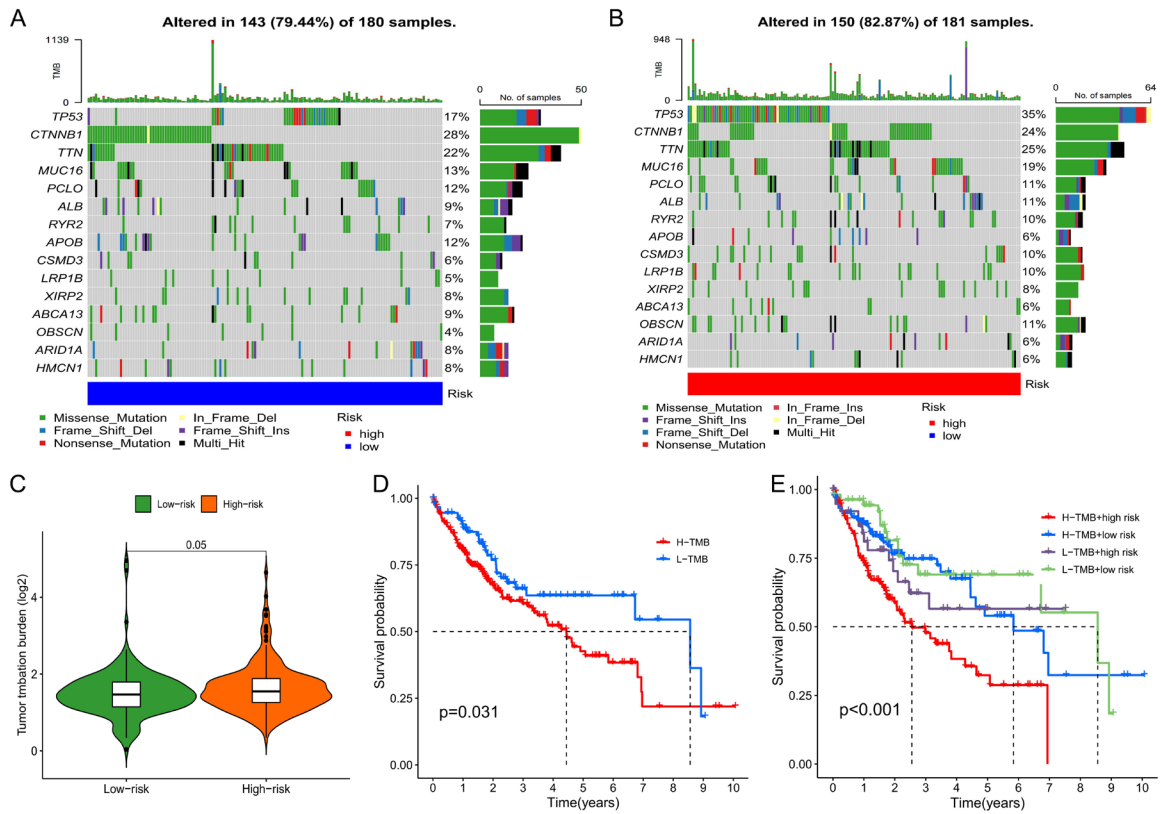
Cuproptosis-related signatures predicted prognosis of HCC

Supplementary Figure 3. Principal component analysis. PCA analysis of all genes (A), all cuproptosis-related genes (B), all cuproptosis-related lncRNAs/mRNAs (C), and cuproptosis-related signatures (D) to explore the differences between high- and low-risk patients.



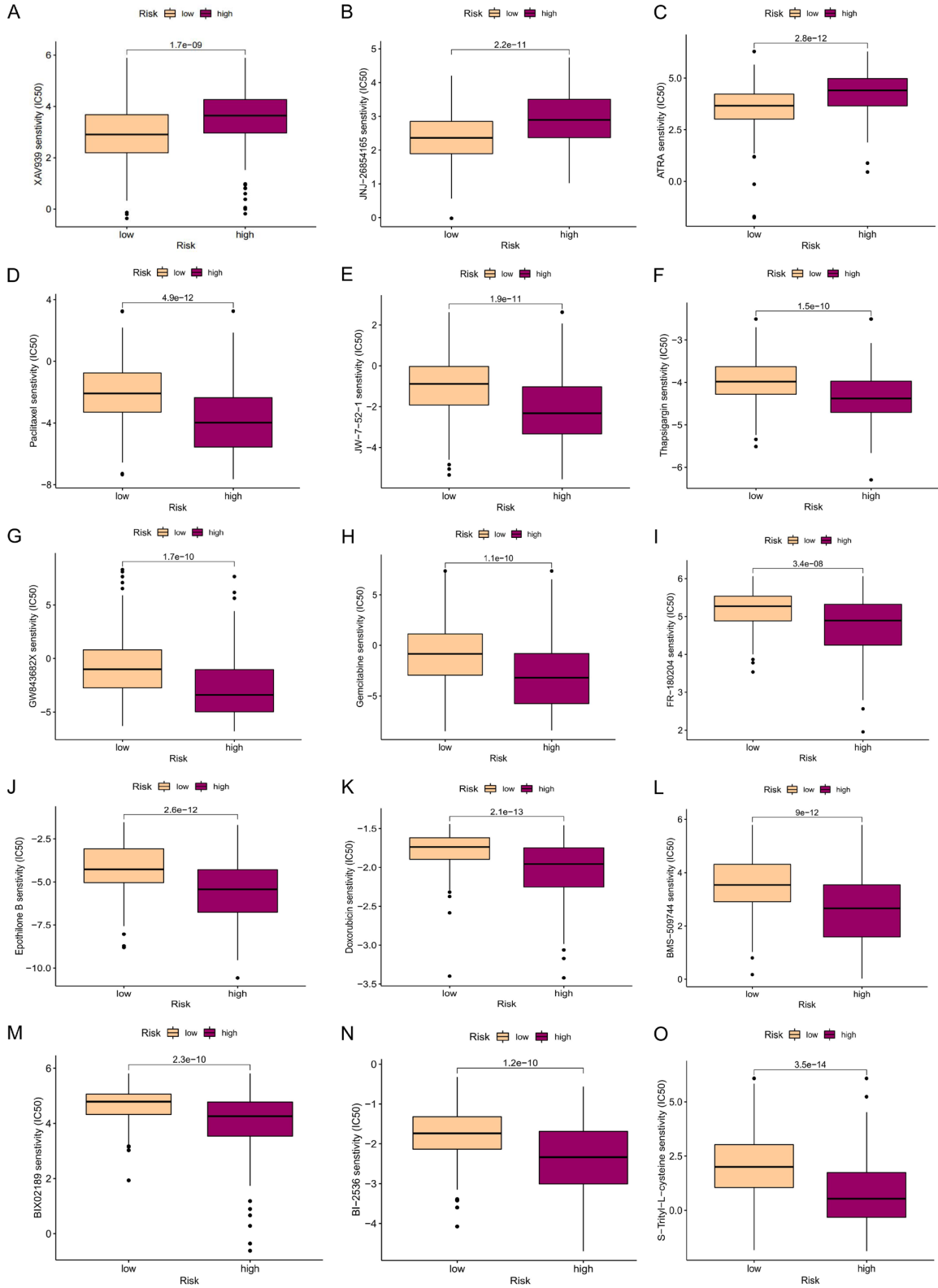
Supplementary Figure 4. Functional and pathway enrichment analysis. (A-C) Histogram (A), bubble plot (B), and circle plot of GO enrichment analysis (C) showed 30 cellular functions that were significantly associated with risk genes and the gene enrichment on each function. (D-F) Histogram (D), bubble plot (E), and circle plot of KEGG enrichment analysis (F) showed 30 pathways that were significantly associated with different risk genes and the number of genes enriched on each pathway.

Cuproptosis-related signatures predicted prognosis of HCC



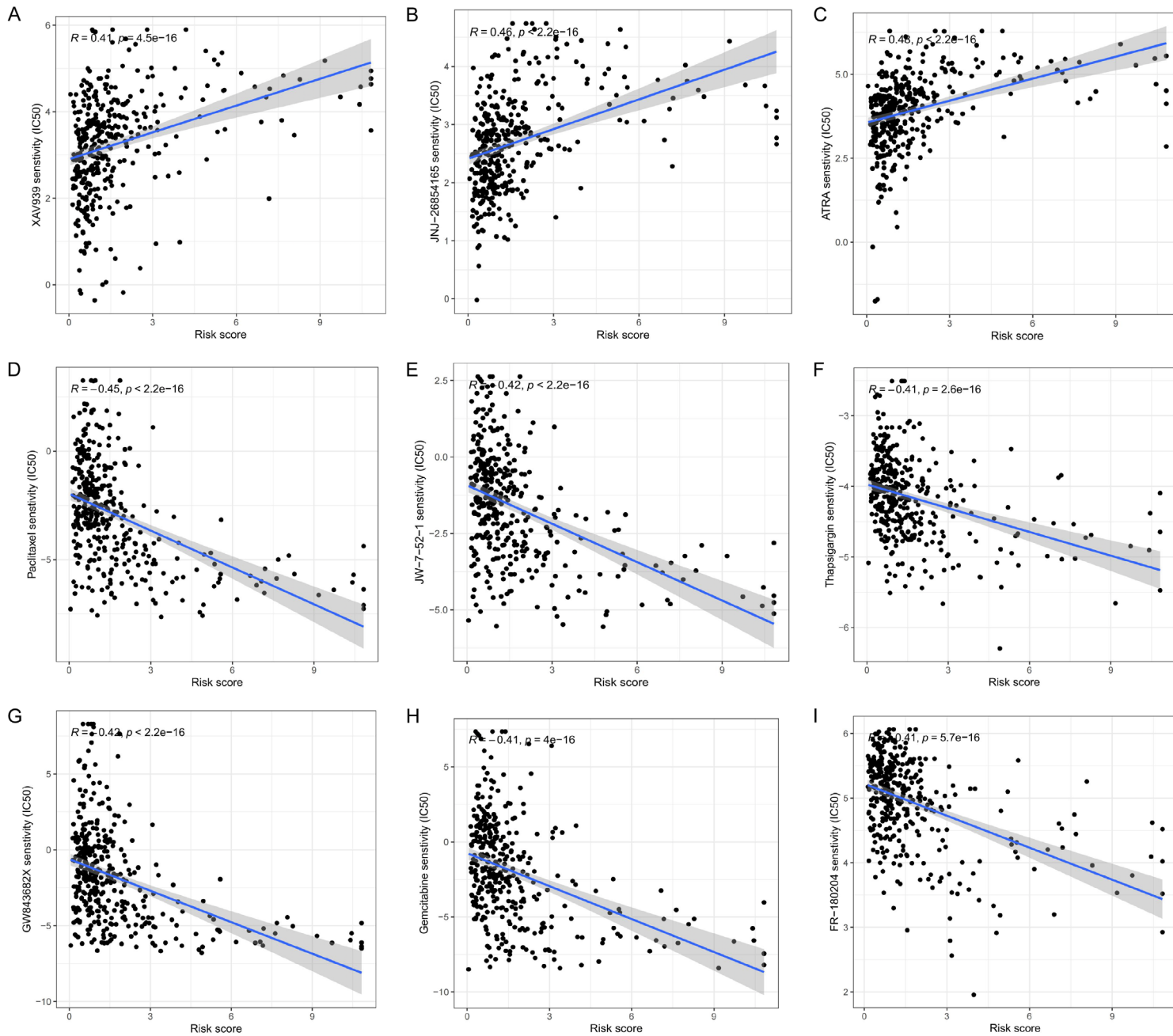
Supplementary Figure 5. Tumor mutational burden analysis. Waterfall plots of 15 genes with the highest mutation frequency in HCC patients in the high- (A) and the low-risk (B) groups. (C) Violin plot of differential analysis of the TMB high- and low-risk groups. (D) Survival analysis curves for the high- and low-TMB groups. (E) K-M analysis curves for the high- and low-TMB combined risk score.

Cuproptosis-related signatures predicted prognosis of HCC

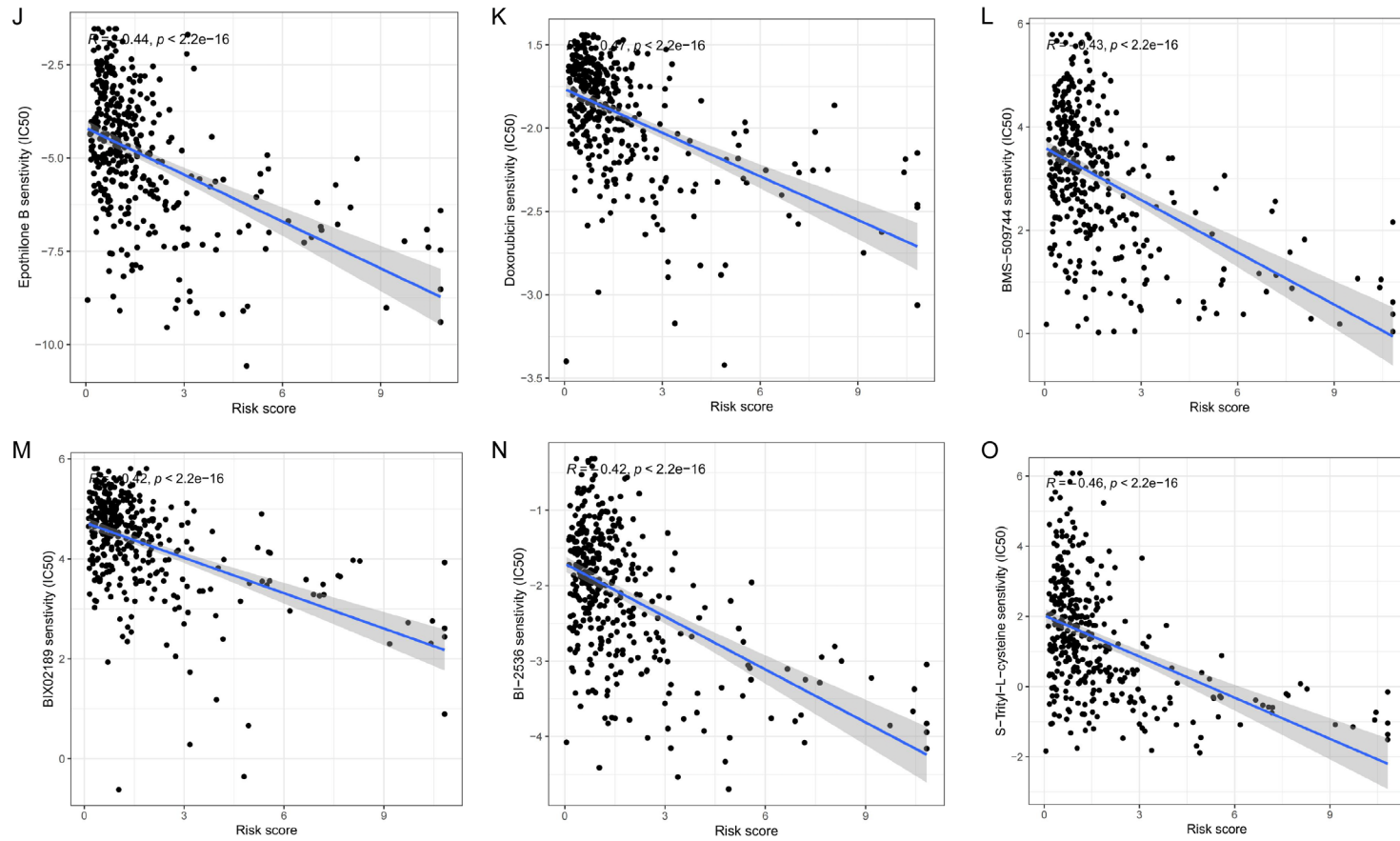


Supplementary Figure 6. Drug sensitivity analysis of the high- and low-risk groups using the prognostic models. The predicted IC50 value of the drugs screened. A. XAV939; B. JNJ-26854165; C. ATRA; D. Paclitaxel; E. JW-7-52-1; F. Thapsigargin; G. GW843682X; H. Gemcitabine; I. FR-180204; J. Epothilone; K. Doxorubicin; L. BMS-509744; M. BIX02189; N. BI-2536; O. S-Trityl-L-cysteine.

Cuproptosis-related signatures predicted prognosis of HCC



Cuproptosis-related signatures predicted prognosis of HCC



Supplementary Figure 7. Correlation analysis between the risk score and drug sensitivity in the prognostic model. A. XAV939; B. JNJ-26854165; C. ATRA; D. Paclitaxel; E. JW-7-52-1; F. Thapsigargin; G. GW843682X; H. Gemcitabine; I. FR-180204; J. Epothilone; K. Doxorubicin; L. BMS-509744; M. BIX02189; N. BI-2536; O. S-Trityl-L-cysteine.